Apparent and inherent optical properties of turbid estuarine waters: measurements, empirical quantification relationships, and modeling

David Doxaran, Nagur Cherukuru, and Samantha J. Lavender

Spectral measurements of remote-sensing reflectance (Rrs) and absorption coefficients carried out in three European estuaries (Gironde and Loire in France, Tamar in the UK) are presented and analyzed. Typical Rrs and absorption spectra are compared with typical values measured in coastal waters. The respective contributions of the water constituents, i.e., suspended sediments, colored dissolved organic matter, and phytoplankton (characterized by chlorophyll-*a*), are determined. The Rrs spectra are then reproduced with an optical model from the measured absorption coefficients and fitted backscattering coefficients. From Rrs ratios, empirical quantification relationships are established, reproduced, and explained from theoretical calculations. These quantification relationships were established from numerous field measurements and a reflectance model integrating the mean values of the water constituents' inherent optical properties. The model's sensitivity to the biogeochemical constituents and to their nature and composition is assessed.

OCIS codes: 010.0010, 010.4450, 010.7340, 000.2170, 120.0280.

1. Introduction

Estuaries are coastal zones that are directly affected by human activities (global warming, pollution, dredging, and intensive fishing), so their study is crucial for preventing long-term damage to coastal waters. Efficient monitoring tools may be developed in such areas by use of ocean color remote sensing,[1,2] whose development of algorithms and validation involves apparent and inherent optical property (AOP and IOP, respectively) field measurements. In coastal waters, these properties are complex and exhibit strong variations, especially in estuaries that are direct sources of terrestrial inputs to the ocean. This explains the absence of a global ocean color algorithm for coastal waters and the development of regional empirical algorithms associated with limited spatial and temporal applications.[3] In highly turbid coastal waters, empirical relationships have been established to quantify the suspended particulate matter successively in the Gironde (France),[4–6] Loire (France),[6] and Tamar (UK)[7] estuaries by use of remote-sensing reflectance (Rrs) ratios. In the Tamar estuary, relationships based on Rrs ratios were also used to quantify the colored dissolved organic matter (CDOM).[7] These relationships proved to be robust (i.e., valid for long-term periods of at least several years).[6] To develop an operational use of ocean color remote-sensing data in turbid waters (e.g., rivers, estuaries, and river plumes), the next logical step is to calibrate, validate, and then use an optical model. Such a model would relate the Rrs signal to the IOPs (e.g. absorption, scattering coefficients) of the water body and then progressively to the chemical and physical characteristics of the water's constituents (concentration, composition, size). It would first be used for a full understanding of the respective influence and contributions of the various water constituents in terms of IOPs and water color. It could then be used to develop quantification relationships directly based on the mean IOPs of a regional area (IOPs measured or derived from the characteristics of the water constituents). Such data could significantly limit the number of costly field campaigns necessary to establish empirical relationships. A special interest also concerns the quantification of chlorophyll-*a* (Chla) concentrations in estuarine waters dominated by terrestrial inputs.

When this research was performed, D. Doxaran was with the Centre for Applied Marine Sciences, University of Wales Bangor, Menai Bridge LL59 5AB, Anglesey, UK. He (doxaran@obs-vlfr.fr) is now with the Laboratoire d'Océanographie de Villefranche, Unité Mixte de Recherche 7093, B.P. 8, 06238 Villefranche-sur-mer Cedex, France. N. Cherukuru is with the Remote Sensing Group, Plymouth Marine Laboratory, Plymouth PL1 3DH, Devon, UK. S. J. Lavender is with the School of Earth, Ocean, and Environmental Sciences, University of Plymouth, Plymouth PL4 8AA, Devon, UK.

Received 16 June 2005; revised 26 September 2005; accepted 30 September 2005.

0003-6935/06/102310-15$15.00/0

Table 1. Details of *In Situ* Measurements

Property Measured	Site of Measurement		
	Gironde Estuary	Loire Estuary	Tamar Estuary
Year (season)	1996–2001 (all seasons)	2002 (winter)	2003–2004 (all seasons)
AOP Instrument (below or above water)	Spectron SE-590 (above)	Spectron SE-590 (above)	Trios RAMSES (above and below)
Number of stations at which AOPs were measured	150	65	50 (above) 150 (below)
TSM			
min./max. (mg l^{-1})	6/2000	30/2600	2/800
Number of stations	150	65	200
Chla			
min./max. (μg l^{-1})	0.1/5	0.1/5	0.4/48
Number of stations	25	10	31
Number of stations at which particle absorption was measured	10		40
Number of stations at which CDOM absorption was measured	30		200

In this study, spectral measurements of Rrs and the absorption coefficient were carried out within two European estuaries: Tamar (UK) and Gironde (France). Additional Rrs measurements were carried out in a third estuarine environment: Loire (France). The objectives were

- To analyze and model the optical properties of turbid estuarine waters and compare them with published values from coastal waters,
- In one representative study area, to quantify the respective contributions of the biogeochemical constituents [nonalgal particles (NAP_l), CDOM, and Chla] to the water's optical signal,
- To calibrate and validate an optical model by use of available IOP and AOP measurements, and
- To reproduce with the model empirical NAP, CDOM, and Chla quantification relationships previously established.

The measured Rrs spectra are reproduced with a bio-optical model, with the measured absorption (a) and predicted backscattering (b_b) coefficients as inputs. The model's sensitivity to the water constituents and to their nature and composition is assessed. The conditions in which the concentrations of the various constituents can be estimated are analyzed, with particular interest in the detection and quantification of Chla. The Rrs signal is then related to the biogeochemical concentrations, and empirical relationships are established, reproduced, and explained from theoretical calculations.

2. Measurements and Analyses

A. Sampling Dates and Locations

Details of the *in situ* measurements are summarized in Table 1.

1. Apparent Optical Properties

In situ radiometric measurements were carried out in three European estuarine environments (Fig. 1): the Gironde estuary (southwestern France) from 1996 to 2001, with a total of 150 stations[4–6]; the Loire estuary (western France) in 2002, with 65 stations[6]; and the Tamar estuary (southwestern UK) in 2003 and 2004, with 200 stations.[7,8] Data were representative of the main parts of the estuaries, from the mouth to the upstream part, but also of different environmental (tidal and seasonal) and illumination (Sun angle and cloud cover) conditions.

2. Water Constituents' Concentrations

The concentration of total suspended matter (TSM, in milligrams per liter) was systematically measured. The Chla concentration (in micrograms per liter) was only occasionally measured in the Gironde and Loire estuaries; in the Tamar estuary Chla measurements

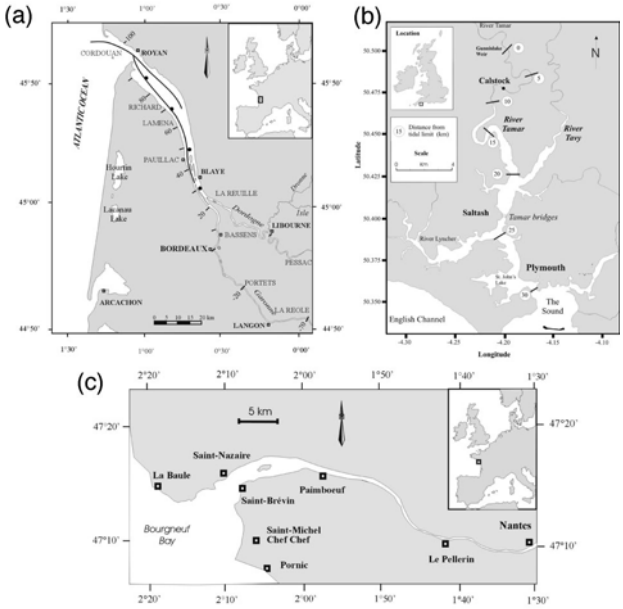

Fig. 1. Maps of the three study areas: (a) Gironde, (b) Tamar, and (c) Loire estuaries.

were systematically carried out during spring–summer of 2004 (a total of 31 stations).

3. Inherent Optical Properties

The Absorption coefficient of CDOM, a_y (in inverse meters at 440 nm), was systematically measured in the Tamar estuary and occasionally in the Gironde. Absorption coefficients of TSM, Chla, and NAP were measured in the Gironde and Tamar estuaries during the 2003–2004 winter periods and in the Tamar estuary during the 2004 spring–summer period.

B. Measurement Techniques and Analyses

1. Apparent Optical Properties

The Rrs signal (in inverse steradians) is defined as the ratio of the water-leaving radiance [L_w (W m^{-2} sr^{-1} nm^{-1})] to downwelling irradiance just above the water's surface [$E_d(0^+)$(W m^{-2} nm^{-1})].[9] Hyperspectral (380–950 nm) radiometric measurements were carried out with a Spectron SE-590 radiance sensor (6° field of view) from 1996 to 2002, a Trios RAMSES-ARC radiance sensor (7° field of view, 350–950 nm), and a Trios RAMSES-ACC-VIS irradiance sensor from 2003 to 2004. $E_d(0^+)$ was measured either directly with irradiance sensor or indirectly with the radiance sensor and a Spectralon reference panel (Labsphere so:9917 and SRT-99-050, respectively).[4,7,10] L_w was initially determined from above-water upwelling radiance measurements (L_t) corrected for surface reflection effects by subtraction of a certain percentage (ρ) of the measured sky radiance signal (L_s).[4–6] The resultant corrections proved to be unsatisfactory in some cases, and an in-water technique was then preferably used. In this case, upwelling radiance (L_u') measurements were recorded at different depths (z) within the first meter below the water's surface[7,8] and then corrected by application of an immersion factor (F_i) to take into account the difference in refractive index between instrument–air and instrument–water[11]:

$$L_u(z, \lambda) = F_i(\lambda) L_u'(z, \lambda), \tag{1}$$

where λ is the wavelength (350 nm $< \lambda <$ 950 nm).

The upwelling radiance just below the water's surface, $L_u(0^-, \lambda)$ and the upwelling radiance attenuation coefficient [K_{L_u} (in inverse meters)] were obtained according to the exponential law[12]

$$L_u(z, \lambda) = L_u(0^-, \lambda) \exp[-K_{L_u}(\lambda)^* z]. \tag{2}$$

We then obtained a first water-leaving radiance signal (L_w') by taking into account mean refraction and reflection effects at the water–air interface[13]:

$$L_w'(\lambda) \approx 0.544 L_u(0^-, \lambda). \tag{3}$$

The L_w' signal was finally corrected for self-shading effects induced by the optical sensor. The measurement error that is due to these self-shading effects, i.e., the difference ε between the measured and the true upwelling radiance signals (denoted L_u^m and L_u^t, respectively), is as a first approximation a function of the radius (r, in meters) of the cylindrical optical sensor and of K_{L_u} according to[14]

$$\varepsilon(\lambda) = 1 - \exp[-k K_{L_u}(\lambda)^* r], \tag{4}$$

where $k = 2/\tan(\theta_{0w})$, θ_{0w} is the in-water refracted solar zenith angle, and $r = 0.0235$ m for a Trios RAMSES-ARC radiance sensor.

Error ε, determined from the measured K_{L_u} coefficient and the calculated θ_{0w} angle, was used to determine L_w as[14]

$$L_w(\lambda) = L_w'(\lambda)/[1 - \varepsilon(\lambda)]. \tag{5}$$

The measured K_{L_u} coefficients logically increased with increasing water turbidity [Figs. 2(a)–2(c)], resulting in high ε errors [Figs. 2(d)–2(f)], notably at short wavelengths (<500 nm) and in the near-infrared domain (700–900 nm). But spectral variations of ε from 500 to 900 nm tend to decrease with increasing water turbidity [Fig. 2(f)]. Above-water optical measurements (L_t and L_s) were usually carried out just before and just after in-water L_u measurements.[8] Consequently, the resultant L_w' and L_w spectra could be compared to above-water upwelling radiance measurements (L_t) corrected for surface reflection effects [$L_t - \rho L_s$]; Figs. 2(g)–2(i). Comparisons proved to be satisfactory when measurements carried out under homogeneous skies, i.e., when ρ was not spectrally dependent, were considered.[9] However, the in-water measurement technique reached its limit in highly turbid waters (TSM $>$ 300 mg l^{-1}) where the L_u signal measured deeper than 0.01 m was negligible (i.e., equal to zero or even slightly negative). In this case, we used above-water measurements to determine L_w.

2. Water Constituents' Concentrations

To determine the TSM concentration we filtered surface water samples through previously weighted filters (Whatman GF/F filters). The filters were then dried and reweighed. We systematically measured two to three replicas to check the uncertainty of the measured TSM concentration (±5%).

For pigment analyses, water samples were filtered in the dark just after collection (Whatman GF/F filters) and kept in a freezer at −20 °C for less than two weeks. Chla concentrations were measured with a Hitachi F-4500 fluorescence spectrophotometer.[15] The observed TSM concentrations were systematically at least one thousand times greater than the Chla concentrations (Table 1). The measured TSM concentrations were consequently assumed also to be representative of the NAP concentrations (NAP_c, in milligrams per liter), as a first approximation.

3. Inherent Optical Properties

Immediately after collection, water samples were filtered through Whatman Anodisc filters (pore size,

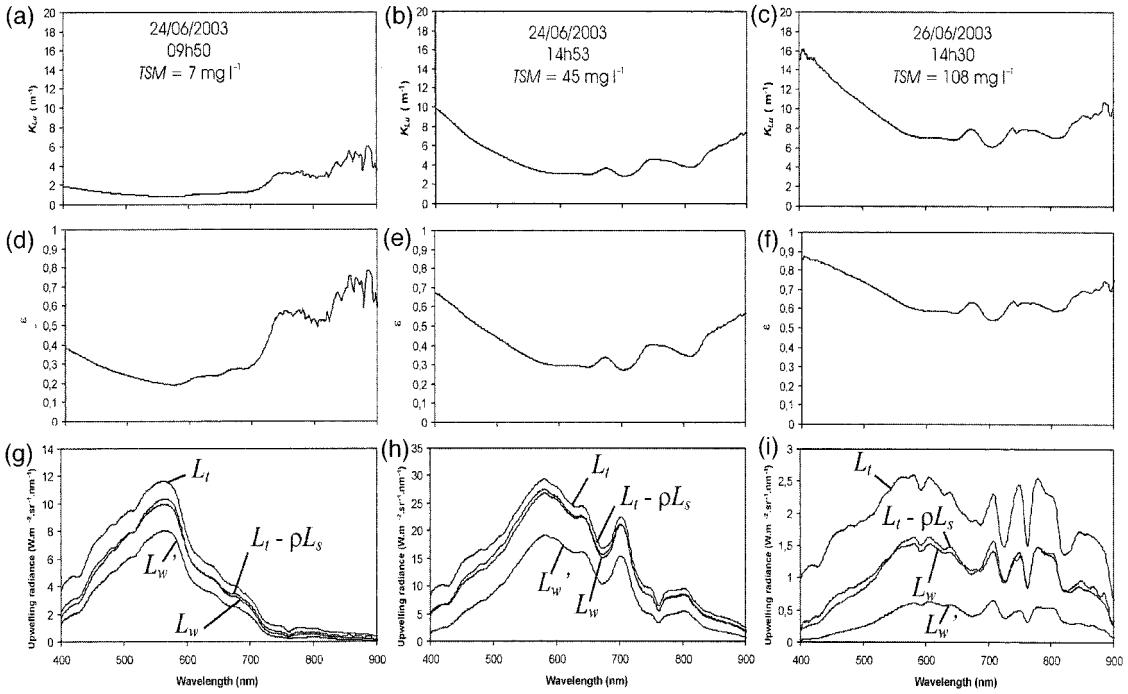

Fig. 2. (a)–(c) Examples of spectral K_{L_u} coefficients determined from in-water L_u measurements carried out in the Tamar estuary on dates and at local times shown. The TSM concentrations are (a) 6.9, (b) 13.1, and (c) 56.6 mg 1^{-1} and the sky conditions are blue, blue, and covered homogeneous, respectively. (d)–(f), Resultant ε errors calculated from Eq. (4). (g)–(i) The respective L_w' and L_w signals (i.e., before and after correction for self-shading effects) are compared to the above-water L_t and $(L_t - \rho L_s)$ signals (i.e., before and after correction for surface reflection effects).

0.20 μm) for CDOM analyses. The residual samples were collected in cleaned glass bottles and stored in a cool box before laboratory analysis; they were then allowed to reach ambient temperature before their absorbance spectra [$\text{abs}_y(\lambda)$, $400 < \lambda < 700$ nm] were measured with a Unicam single-beam spectrophotometer (5 cm path-length cuvette). We recorded an absorbance spectrum of Milli-Q water [$\text{abs}_{\text{MQ}}(\lambda)$] before and after the sample measurement to check the stability of the lamp. The CDOM absorption coefficient was calculated according to[16]

$$a_y(\lambda) = 2.303[\text{abs}_y(\lambda) - \text{abs}_{\text{MQ}}(\lambda)]/l, \tag{6}$$

where l (in meters) is the path length of the cuvette.

Just after collection, water samples were filtered (Whatman GF/F filters; diameter, 25 mm) for analyses of particulate absorption. Filters were stored in liquid nitrogen for as much as six weeks before analysis in the laboratory. The phytoplankton (a_c) and NAP (a_s) absorption coefficients were determined from 350 to 750 nm on a Perkin-Elmer Lambda 800 spectrophotometer retrofitted with a 60 mm Spectralon coated integrating sphere by a method adapted to turbid waters.[17,18]

3. Optical Model

A. Model Description

A simplified bio-optical model was selected for use in this study. In infinitely deep water or turbid waters for which any bottom effect can be ignored, Rrs can be related to the IOPs according to[19]

$$\text{Rrs} = \frac{0.176}{Q(\lambda)} \frac{b_b(\lambda)}{a(\lambda) + b_b(\lambda)}, \tag{7}$$

with 0.176 resulting from an empirical coefficient and approximation of air–water transmission effects and where Q is the ratio of upwelling irradiance to upwelling radiance (a constant value Q of 3.6 sr is considered in this study).[20] The total absorption and backscattering coefficients of the water body, a and b_b (in inverse meters), can be written as the sums of the contributions of the various water constituents:

$$a(\lambda) = a_w(\lambda) + a_y(\lambda) + a_s(\lambda) + a_c(\lambda), \tag{8}$$

$$b_b(\lambda) = b_{\text{bw}}(\lambda) + b_{\text{bs}}(\lambda) + b_{\text{bc}}(\lambda), \tag{9}$$

where subscripts w, y, s, and c, respectively, correspond to water, CDOM, NAP, and Chla. Values of $a_w(\lambda)$ in the visible spectral domain (380–730 nm) and at near-infrared wavelengths (730–950 nm) were taken from the literature.[21,22]

Absorption of light by CDOM and NAP was modeled with a similar exponential law decreasing with increasing wavelength[23]:

$$a_{y/s}(\lambda) = a_{y/s}(440)\exp[-k_{y/s}(\lambda - 400)], \tag{10}$$

where $a_y(440)$ is representative of the CDOM concentration. The NAP absorption, $a_s(440)$, can be written as $\mathrm{NAP}_c \times a_s^*(440)$, where $a_s^*(440)$ is the mass specific absorption coefficient of NAP. Coefficient $k_{y/s}$ depends on the composition of the dissolved–suspended matter. The chlorophyll absorption, $a_c(\lambda)$, is written as Chla $\times$ $a_c^*(\lambda)$, where a_c^* is the mass specific absorption coefficient of Chla.

The backscattering of water, $b_{bw}(\lambda)$, was taken as half the scattering values of water molecules available in the literature.[24] The backscattering of chlorophyll, $b_{bc}(\lambda)$, is written as Chla $\times$ b_{bc}^*, where b_{bc}^* is the mass specific backscattering coefficient of Chla taken from Lahet *et al.*[25] Finally, the backscattering coefficient of NAP is written as[26]

$$b_{bs}(\lambda) = \mathrm{NAP}_c \times b_{bs}^*(550)\left(\frac{\lambda}{550}\right)^{-\gamma}, \qquad (11)$$

where $b_{bs}^*(550)$ is the mass specific coefficient of NAP at 550 nm; the γ exponent can be directly related to the particle grain-size distribution.[27]

B. Model Calibration

In situ and laboratory IOP measurements but also literature information was used to calibrate the bio-optical model, i.e., to determine the unknown parameters in Eqs. (8) and (9).

1. *Absorption Coefficients*

Based on CDOM absorption measurements available and on literature information,[28,29] $a_y(440)$ and k_y were considered constant and equal to, respectively, 0.1 m^{-1} and 0.017 nm^{-1} in the Gironde and 0.5 m^{-1} and 0.017 nm^{-1} in the Loire estuaries. In the Tamar estuary the measured $a_y(\lambda)$ and k_y values were considered in the model.

When available, the measured values of absorption by particles were used within the model. When they were not available, the ranges of $a_s^*(440)$ and k_s considered were determined from mean values (available measurements) and literature information:[23,30] 0.025–0.070 $\mathrm{m}^2\,\mathrm{g}^{-1}$ and 0.006–0.015 nm^{-1}, respectively.

Chlorophyll concentrations and $a_c^*(\lambda)$ were used within the model if they were measured; when they were not, mean $a_c^*(\lambda)$ values taken from Lahet *et al.*[25] were used. A constant Chla concentration of 0.5 $\mu\mathrm{g}\,\mathrm{l}^{-1}$ was assumed to be representative of the Gironde and Loire estuaries independently of season[29] but only during the winter period of the Tamar estuary,[31] as some seasonal measurements were available.

2. *Backscattering Coefficients*

No $b_{bs}(\lambda)$ measurements were available for this study. We used Eq. (11) to model this parameter by considering typical variations for $b_{bs}^*(550)$ and γ. Babin *et al.*[26] have given typical mass specific scattering coefficients for NAP from various European coastal waters, $b_s(\lambda)$, in the range 0.42–0.56 $\mathrm{m}^2\,\mathrm{g}^{-1}$. By assuming that the Petzold function can be applied for turbid waters,[32] we took $b_{bs}(\lambda)$ to be 0.019 times $b_s(\lambda)$, which resulted in the following variation range: 0.007–0.011 $\mathrm{m}^2\,\mathrm{g}^{-1}$. Based on recent computations,[26] a range of 0–1 in γ was considered.

To calibrate the model we initially considered field stations where CDOM and NAP absorption coefficients were available. The difference between the measured and the modeled Rrs signals (denoted $\mathrm{Rrs}^{\mathrm{meas}}$ and $\mathrm{Rrs}^{\mathrm{model}}$, respectively) was written as

$$\mathrm{Diff\_Rrs} = \sum_{i=1}^{n}\left[\left(\mathrm{Rrs}^{\mathrm{model}}(\lambda_i) - \mathrm{Rrs}^{\mathrm{meas}}(\lambda_i)\right)/\mathrm{Rrs}^{\mathrm{meas}}(\lambda_i)\right], \qquad (12)$$

where λ_1 and λ_n are the limits of the spectral range considered. Using the measured water constituents' concentrations and absorption coefficients, the general method was to minimize Diff_Rrs by fitting the $b_{bs}(\lambda)$ values, i.e., by fitting the unknown $b_{bs}^*(550)$ and γ values in Eq. (11). This gave an overview of the IOP variations and mean values in the Gironde and Tamar estuaries. The full data set was then considered (including the stations with no IOP measurement available). The mean IOP values previously determined (Table 2) were first selected in the model (the Loire mean IOP values were assumed here to be similar to those determined in the Gironde) and then fitted to reproduce the measured Rrs spectra. The (600–900, 500–600, and then 400–500 nm spectral ranges were successively considered to fit the $b_{bs}^*(550)$ and γ values; then, if those values were not available, $a_s^*(440)$ and k_s.

4. Results

A. Inherent Optical Properties

The IOP values and variations observed in the three estuaries are summarized in Table 2. The $a_y(\lambda)$ measurements consistently agreed with Eq. (10), with k_y values in the 0.017 $\pm$ 0.005 nm^{-1} range [Fig. 3(a)]. Within the 400–650 nm spectral range, Eq. (10) reproduced the $a_y(\lambda)$ measurements with a determination coefficient of at least 0.9. The $a_c^*(\lambda)$ Tamar measurements [Fig. 3(b)] were similar to those recently observed in the English Channel.[23] This result could be expected in the downstream part of the estuary and adjacent Plymouth Sound waters but would be unexpected in the upstream part of the estuary, where freshwater phytoplankton species are usually predominant.[33]

The NAP absorption measurements generally agreed with Eq. (10), where $a_s^*(440)$ and k_s were in the 0.0225 $\pm$ 0.015 $\mathrm{m}^2\,\mathrm{g}^{-1}$ and 0.0125 $\pm$ 0.008 nm^{-1} ranges, respectively, in the Tamar [Fig. 3(c)] and in the 0.016 $\pm$ 0.003 $\mathrm{m}^2\,\mathrm{g}^{-1}$ and 0.0122 $\pm$ 0.004 nm^{-1} ranges in the Gironde [Fig. 3(d)] estuaries. An exponential increase of $a_s^*(\lambda)$ at wavelengths shorter than 700 nm was thus observed, which had a slope that closely agreed with recent measurements carried out in various European coastal waters.[23] Considering the 400–750 nm spectral range, Eq. (10) reproduced

Table 2. Details of the Measured and Modeled IOPs in the Three Estuaries[a]

IOP	Gironde Estuary (min./mean/max.)	Loire Estuary (min./mean/max.)	Tamar Estuary (min./mean/max.)
$a_y(440)$ (m^{-1})	0.05/0.15/0.26	*0.05/0.15/0.26*	0.04/0.59/3.63
k_y (nm^{-1})	0.015/0.017/0.020	*0.015/0.017/0.020*	0.012/0.017/0.022
a_s*(440) ($m^2\ g^{-1}$)	0.013/0.016/0.019	*0.013/0.016/0.019*	0.010/0.025/0.040
k_s (nm^{-1})	0.008/0.012/0.016	*0.008/0.012/0.016*	0.005/0.013/0.021
$a_c(443)$ ($m^2\ mg^{-1}$)	0.0024/0.048/0.093	*0.0024/0.048/0.093*	0.030/0.048/0.090
a_c*(675) (m^{-1})	0.004/0.012/0.024	*0.004/0.012/0.024*	0.013/0.023/0.059
b_{bs}*(550) ($m^2\ g^{-1}$)	*0.008/0.011/0.011*	*0.007/0.011/0.011*	*0.008/0.010/0.011*
γ	*0.0/0.4/1.0*	*0.0/0.1/1.0*	*0.0/0.0/0.9*
b_{bc}*(550) ($m^2\ mg^{-1}$)	*0.0004*	*0.0004*	*0.0004*
b_{bc}*(685) ($m^2\ mg^{-1}$)	*0.0006*	*0.0006*	*0.0006*

[a]The values taken from the literature (i.e., not measured) and used in the optical model are indicated by italics. For each parameter, the minimum and maximum values give the range observed or used to reproduce the measured Rrs spectra. The mean value is the one used in the model when the empirical quantification relationships, i.e., the value that is most representative of each whole estuary, are reproduced. Note that no IOP measurement was performed in the Loire estuary and that IOP values were taken from the IOPs measured in the Gironde estuary.

the $a_s(\lambda)$ measurements with a determination coefficient of at least 0.95. However, specific spectral variations (absorption peaks and troughs) were also detected near 500 nm, which could indicate the absorption of iron minerals.[34] Further investigation is needed to confirm and explain these observations.

Recent Mie calculations suggest a high variability of a_s*(440) in seawater, depending on the composition of the mineral particles,[35] with coastal *in situ* measurements confirming this statement.[23,30] The a_s*(440) values measured in both estuaries appear to be close to (though slightly lower than) those observed in the Irish Sea[30] and significantly lower than those observed in various coastal waters (mean value of 0.041 $m^2\ g^{-1}$, or 0.036 $m^2\ g^{-1}$ when data collected in the Baltic Sea are excluded).[23] It is expected that inorganic particles will have lower a_s*(440) values than organic particles,[23] which can explain the observations made, as both estuaries were dominated by mineral suspended matter. A high a_s*(440) variability was observed in the Tamar estuary, where the TSM organic content typically varied from 10% (upstream) to 90% (mouth). A low variability was observed in the Gironde estuary, where the TSM organic content is generally low and stable.[29] Further investigation is needed to determine the influence of NAP organic content on NAP light-absorption properties.

Both the Gironde and the Tamar estuaries have high NAP concentrations, and NAP backscattering

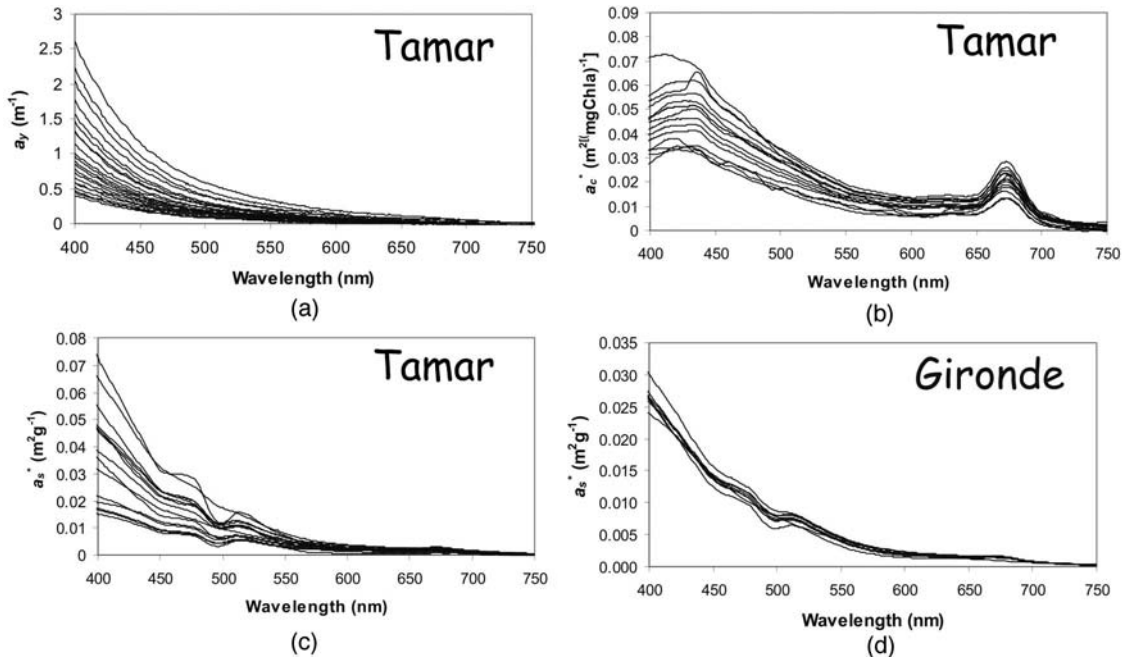

Fig. 3. Typical absorption coefficients: (a) a_y, (b) a_c*, and (c) a_s* spectra measured in the Tamar estuary. (d) Typical a_s* spectra measured in the Gironde estuary.

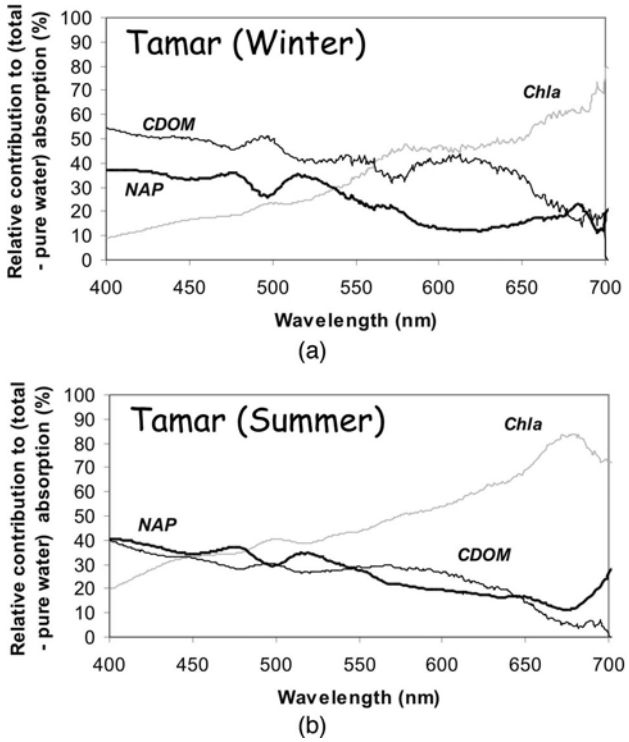

Fig. 4. Relative contributions of CDOM, NAP, and Chla to the (total − pure water) absorption signal in the Tamar estuary during winter and summer.

properties were assumed to be dominant in the total backscattering signal, as a first approximation.[36] However, for absorption of light, CDOM absorbs significantly at short wavelengths (<500 nm) and Chla has absorption peaks near 443 and 675 nm.[37] It is therefore important to determine the contribution of each water constituent to the total absorption to highlight the spectral domain where each constituent is dominant. Once identified, specific wavelengths may then be selected to develop a general (NAP, CDOM, and Chla) quantification algorithm. During winter 2003–2004 in the Gironde estuary, the total particulate absorption was high compared with the CDOM contribution: $a_s(\lambda)$ represented more than 90% of the total signal from 350 to 600 nm and more than 60% of the total signal from 600 to 750 nm. It may therefore be difficult to develop winter CDOM quantification algorithms in the Gironde estuary. In the Tamar estuary, NAP and CDOM were dominant during the 2003–2004 winter (October 2003–April 2004) period [Fig. 4(a)], but during spring–summer (May–September) 2004 the relative contribution of Chla greatly increased and became dominant from 550 to 700 nm [Fig. 4(b)]. This result has led to the development of CDOM quantification relationships,[7] and the detection of Chla may also be possible by use of red wavelengths (>600 nm) during spring–summer.

B. Apparent Optical Properties

In the Gironde and Loire estuaries, a typical Rrs signal was observed to increase with increasing TSM concentration: first in the visible, then in the red, and finally in the near-infrared wavelengths [Fig. 5(a)].[4–6] Despite the coexistence of high CDOM and Chla concentrations in the Tamar estuary, similar spectra were observed [Figs. 5(b) and 5(c)]. Note that the artifact usually observed near 760 on the Rrs spectra is due to absorption of light by oxygen molecules and is not related to the water IOPs. The mag-

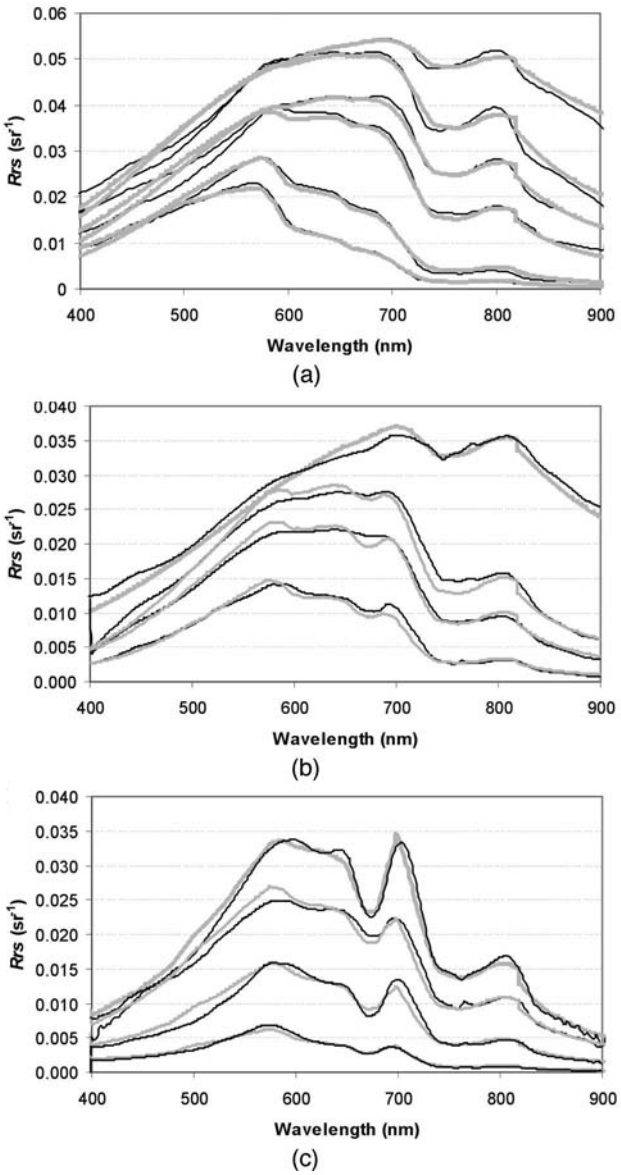

Fig. 5. Typical Rrs spectra measured (darker curves) and reproduced with the optical model (lighter curves) (a) in the Gironde estuary for TSM concentrations of 9, 35, 82, 210, 365, and 837 mg l^{-1} from bottom to top, (b) in the Tamar estuary during the 2003 winter period for TSM concentrations of 19, 44, 69, and 797 mg l^{-1} with $a_y(440)$ values in the range 0.4–1.8 m^{-1} and Chla concentrations lower than 5 μg l^{-1}, and (c) in the Tamar estuary during the 2004 summer period for TSM concentrations of 7, 20, 43, and 59 mg l^{-1} with $a_y(440)$ values in the range 0.5–0.9 m^{-1} and Chla concentrations in the range 15–32 μg l^{-1}. Model inputs are the water constituents' concentrations; measured a_y, a_c, and a_s absorption coefficients; and $b_{bs}{}^*(550)$ and γ values fitted in the ranges 0.007–0.011 m^{-1} and 0–1, respectively.

Table 3. Difference {Diff_Rrs = [(Rrs^{model} − Rrs^{meas})/Rrs^{meas}], in percent} between Modeled and Measured Rrs Signals[a]

	Diff_Rrs (%)			
		Tamar Estuary		
Spectral Bond (nm)	Gironde Estuary	Winter	Spring–Summer	Global
400–500	±4.4	±10.3	±13.3	±11.8
500–600	±4.0	±4.3	±7.7	±6.0
600–700	±1.1	±3.7	±3.2	±3.5
700–800	±7.4	±7.1	±7.8	±7.5
800–900	±7.9	±7.4	±10.0	±8.7
400–900	±4.9	±6.6	±8.4	±7.5

[a]Results are presented for the whole spectral domain considered (400–900 nm) and each enclosed 100 nm wide spectral band. Results obtained for the Loire estuary, which are quite similar to the Gironde results, are not presented, as no IOP measurement was available with which to calibrate the model.

nitude of the Rrs spectra measured was observed to be lower in the Tamar (typically 0–0.035 sr^{-1}) than in the Gironde and Loire estuaries [cf. Figs. 5(b) and 5(c) with Fig. 5(a)],[6] but some of these latest spectra were proved to be overestimated owing to an underestimation of the $E_d(0^+)$ signal determined from measurements of a Spectralon plaque.[10] Moreover, in the Tamar, a seasonal variability was also highlighted with the appearance of a Rrs depression at 675 nm during spring and summer [cf. Fig. 5(c) with Fig. 5(b)]. This depression was systematically detected for high Chla concentrations (from 5 μg to 50 μg l^{-1}) as already observed in turbid productive waters.[38–40]

We systematically reproduced the measured Rrs spectra with the optical model by fitting the b_{bs}*(550) and γ values in Eq. (6). The model reproduced most of the Rrs spectra measured in the Gironde estuary [Fig. 5(a)] with good agreement (Diff_Rrs = ±5% from 400 to 900 nm; Table 3). As the Gironde estuarine waters are sediment dominated, selecting appropriate IOPs for NAP was sufficient to produce satisfactory results. Similar results were obtained for the Loire estuary. However, the model could not reproduce some of the spectra measured in these two estuaries, which exhibited Rrs values greater than 0.10 sr^{-1}.[6] These values were clearly overestimated owing to shadow effects on the Spectralon plaque used to determine $E_d(0^+)$,[10] and they had to be divided by a constant value (i.e., a value from 1 to 2, independently of wavelength)[10] to be reproduced. The model reproduced all the Rrs spectra measured in the Tamar estuary: during winter [Fig. 5(b)] with an agreement (Diff_Rrs) of ±6.6% from 400 to 900 nm (Table 3) and during summer [Fig. 5(c)] with an agreement (Diff_Rrs) of ±8.4% from 400 to 900 nm (Table 3). Results obtained for the Tamar estuary were satisfactory but not so good as for the Gironde, as appropriate IOPs for NAP but also for CDOM and Chla had to be selected.

The use of such wide IOP ranges in the model (Table 2) highlighted the high variability of the water constituents' characteristics (composition and particle grain size). In the Gironde and Loire estuaries, the NAP optical properties appeared to be predominant. In the Tamar, absorption by CDOM proved to be significant at short wavelengths (<500 nm); the depression at 675 nm observed during spring–summer [Fig. 5(c)] was proved to be due to Chla absorption. This phenomenon was clearly observable in highly turbid waters (TSM > 20 μg l^{-1}), as the Rrs signal was significantly greater than zero in the red and near-infrared parts of the spectrum. Thus, if the use of a blue wavelength (e.g., 443 nm) to detect Chla is certainly inappropriate in turbid estuarine waters, the use of a red wavelength (i.e., 675 nm where the influence of CDOM is almost negligible and strong backscattering by TSM leads to positive Rrs values) may be successful.

C. Quantification Relationships

Results are presented with consideration given to spectral wavelengths close to satellite ocean color [Sea-Viewing Wide Field-of-View Sensor (SeaWiFS), Moderate-Resolution Imaging Spectroradiometer (MODIS), and Medium Resolution Imaging Spectrometer (MERIS) bands, so the relationships obtained can easily be adapted and applied to remote-sensing data.

1. *Suspended Particulate Matter*

In the Gironde and Loire estuaries, empirical TSM quantification relationships were established by use of Rrs ratios of a near-infrared (e.g., 850 nm) to a visible (e.g., 550 or 650 nm) wavelength.[6] These robust relationships, established from numerous *in situ* measurements (carried out during a six-year period in the Gironde estuary) were apparently little affected by the IOP tidal and seasonal variations. This assumption would be confirmed if they could be reproduced with the model integrating the mean IOP values. Considering the Gironde estuarine waters as sediment dominated, the contributions of CDOM and Chla were initially ignored, and the mean IOPs were assumed to be due only to pure water and NAP. The result obtained was satisfactory, as the model reproduced the empirical relationships based on the Rrs(850)/Rrs(550) and Rrs(850)/Rrs(650) ratios [Figs. 6(a) and 6(b), respectively] when

- The mean values measured for a_s*(440) and k_s in Eq. (10) were considered and
- Appropriate mean values of b_{bs}* (550) and γ (0.011 m^2 g^{-1} and 0.4 nm^{-1}, respectively) were fitted.

It was thus confirmed that knowing the mean IOP values for NAP is enough to establish TSM quantification relationships in the Gironde estuary. Moreover, it was interesting to use the model to investigate how the respective variations of b_{bs}*(550) and a_s*(440) (mainly related to the NAP composition) may affect these relationships. High b_{bs}*(550) variations (±50%) were considered (0.0055–0.0165 m^2 g^{-1}). As

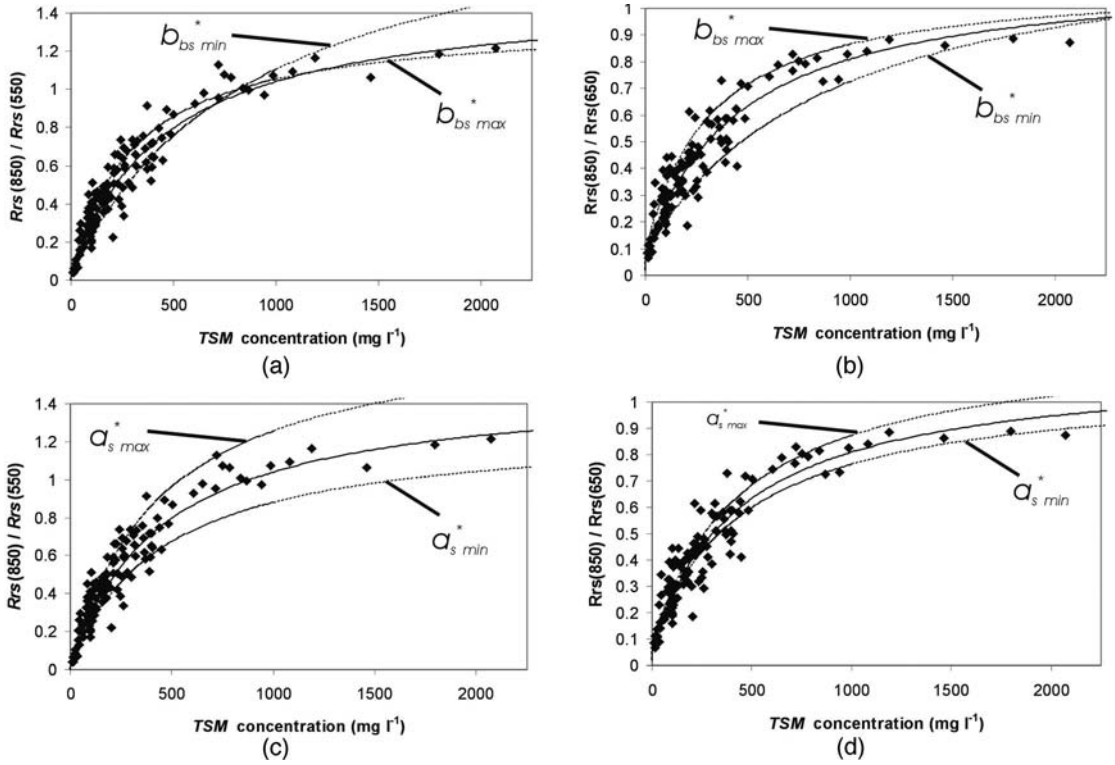

Fig. 6. TSM quantification relationships established in the Gironde estuary for the Rrs(850)/Rrs(550) and Rrs(850)/Rrs(650) ratios. Each point represents a field measurement; a solid curve represents the model results of using mean IOP values (see the text for model parameter details). Dotted curves represent relationships established with the model for (a), (b) ±50% variations of the mean b_{bs}*(550) value and (c), (d), ±50% variations of the mean a_s*(440) value.

expected, the influence on the Rrs(850)/Rrs(550) ratio is quite limited, except at the highest TSM concentrations, for which the actual b_{bs}*(550) value may not vary significantly [Fig. 6(a)]. The influence is higher on the Rrs(850)/Rrs(650) ratio (though this influence is still limited), as the Rrs signal at these wavelengths depends mainly on the backscattering properties of the water body [Fig. 6(b)]. It certainly explains part of the scatter of the points obtained from *in situ* measurements. To illustrate the influence of a_s*(440) variability, we considered ±50% variations about the mean a_s*(440) value (0.0105–0.0215 $m^2\ g^{-1}$). Once again, results show a limited influence on the Rrs ratios [Figs. 6(c) and 6(d)]. This influence is higher for the Rrs(850)/Rrs(550) ratio, as absorption by NAP is significant at 550 nm, and certainly explains part of the scatter of the points obtained from *in situ* measurements [Fig. 6(c)]. It is quite low for the Rrs(850)/Rrs(650) ratio, as absorption by NAP is minimum in the red and near-infrared spectral domains [Fig. 6(d)].

The model was able to reproduce the empirical TSM quantification relationships established in the Loire estuary (Fig. 7) when

- The mean a_s*(440) and k_s values measured in the Gironde estuary [Eq. (10)] were considered and
- Appropriate mean b_{bs}*(550) and γ values (0.011 $m^2\ g^{-1}$ and 0.1 nm^{-1}, respectively), were fitted.

It was then interesting to use the model to determine how the respective va/priations of γ and k_s (related to the composition and size distribution of NAP) may affect these relationships. A wide range (0–1) was considered for the γ values. Once again, the influence of these variations (representative of variations of the NAP size distribution)[26] on both Rrs ratios appeared to be quite limited and was not significantly dependent on the TSM concentration [Figs. 7(a) and 7(b)]. However, it may certainly explain part of the scatter of the points obtained from *in situ* measurements. Strong k_s variations (0.006–0.015 nm^{-1}) were then considered to highlight the potential influence of this parameter. Results show an increasing influence on both Rrs ratios with increasing TSM concentration [Figs. 7(c) and 7(d)], highlighting the important role played by absorption by NAP in highly turbid sediment-dominated waters.

Similar empirical relationships were established in the Tamar estuary (Fig. 8), although the slopes of the relationships obtained were quite different from those for the Gironde and Loire estuaries. Again, the model could closely reproduce these empirical relationships (Fig. 8) when

- The mean values measured for a_s*(440) and k_s in Eq. (5) were considered and
- Appropriate mean values of b_{bs}*(550) and γ (0.008 $m^2\ g^{-1}$ and 0.4 nm^{-1}, respectively) were fitted.

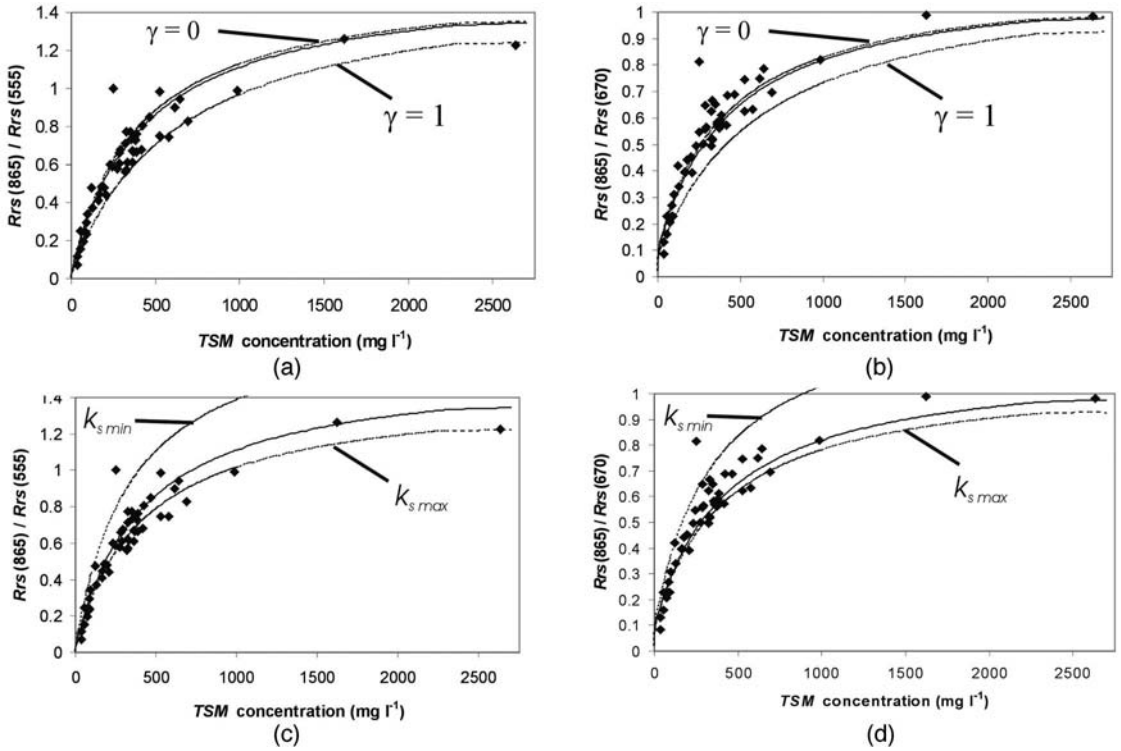

Fig. 7. TSM quantification relationships established in the Loire estuary for the Rrs(865)/Rrs(555) and Rrs(865)/Rrs(670) ratios. Each point represents a field measurement; a solid curve represents the model results of using mean IOP values (see the text for model parameter details). Dotted curves represent the relationships established with the model for (a), (b) variations of γ from 0 to 1 and (c), (d) ±50% variations of the mean k_s value.

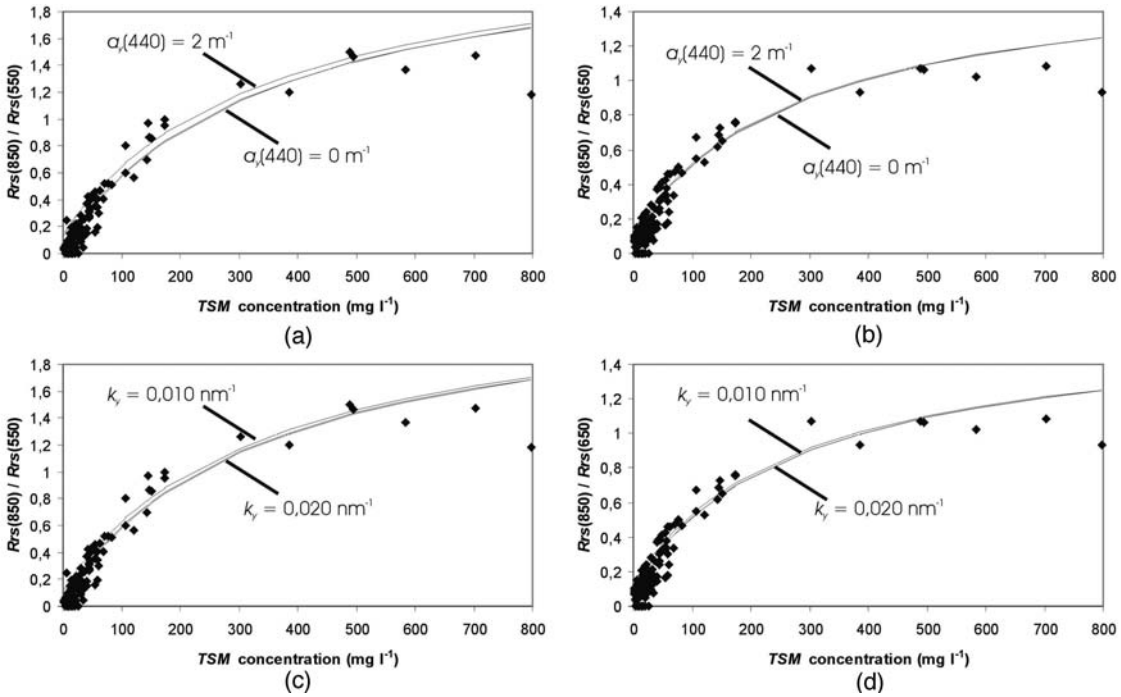

Fig. 8. TSM quantification relationships established in the Tamar estuary for the Rrs(850)/Rrs(550) and Rrs(850)/Rrs(650) ratios. Each point represents a field measurement; a solid curve represents the model results of using mean IOP values (see the text for model parameter details). Dotted curves represent the relationships established with the model for (a), (b) variations of $a_y(440)$ from 0 to 2 m^{-1} and (c), (d) variations of k_y from 0.010 to 0.020 nm^{-1} with a fixed CDOM concentration [$a_y(440) = 1\ m^{-1}$].

Thus, even in the Tamar where high CDOM concentrations were regularly observed, the influence of CDOM optical properties on the Rrs ratios appeared to be extremely limited. This was confirmed when the model was run with different CDOM concentrations $a_y(440)$ in the range 0–2 m^{-1}] and CDOM compositions (k_y values in the range 0.010–0.020 nm^{-1}) for a fixed CDOM concentration [$a_y(440) = 1\ m^{-1}$; Fig. 8]. Only the Rrs(850)/Rrs(550) ratio is slightly influenced by changing CDOM concentrations [as CDOM absorption at 550 nm is not negligible; Fig. 8(a)]. This is not the case for the Rrs(850)/Rrs(650) ratio [Fig. 8(b)]. The influence of CDOM composition variations through the k_s coefficient is almost insignificant [Figs. 8(c) and 8(d).

As a first conclusion, knowledge of NAP optical properties is sufficient to establish TSM quantification relationships in the three estuarine environments. This knowledge may be obtained from numerous *in situ* or laboratory measurements or derived from theoretical calculations based on NAP composition and size.[23,26] The $b_{bs}^*(550)$ values used in the model were in the expected range[26] but still need to be validated with *in situ* measurements.

2. Colored Dissolved Organic Matter

In turbid coastal waters, *in situ* measurements showed that empirical CDOM quantification relationships can be established by use of the Rrs ratio of two visible wavelengths.[41] In the Tamar estuary, both CDOM and TSM concentrations increase from the mouth to the upstream part, but no correlation was observed between the two parameters [Fig. 9(a)]. However, the Rrs ratio from 400 to 700 nm correlated with the CDOM concentration, according to a power law regression with a determination coefficient of 0.87 [Fig. 9(b)].

Considering the mean IOP values for CDOM ($k_y = 0.017\ nm^{-1}$) and NAP (Table 2) and the measured NAP concentrations and ignoring the Chla optical properties allowed the optical model to reproduce the measured Rrs ratio [Fig. 9(c)]. Such was not the case if the measured NAP concentrations were not considered as model inputs, as NAP and CDOM have similar light-absorption properties [Eq. (10)]. The NAP contribution to the Rrs signal was thus generally predominant in the estuary and had to be taken into account initially. The Rrs ratio measured and reproduced by the model globally followed a 1:1 regression, but the points were rather scattered. A better reproduction of the measured ratio would also require the integration of the actual IOP values for CDOM and NAP as model inputs. The mean difference observed between the measured $a_y(440)$ values and the values given by the power law from the Rrs(400)/Rrs(700) ratio [Fig. 9(b)] is ±20%. The difference between the measured Rrs(400)/Rrs(700) ratio and the ratio values calculated by the model [Fig. 9(c)] is ±30%. Consequently, by knowing the mean NAP and CDOM optical properties in a study area, one can estimate the TSM (and thus NAP in the case of sediment-dominated waters) and then CDOM concentrations successively from multispectral Rrs data. Based on our results obtained for Tamar estuary, the retrieved CDOM concentrations will be associated with a cumulative percentage error less than ±50%.

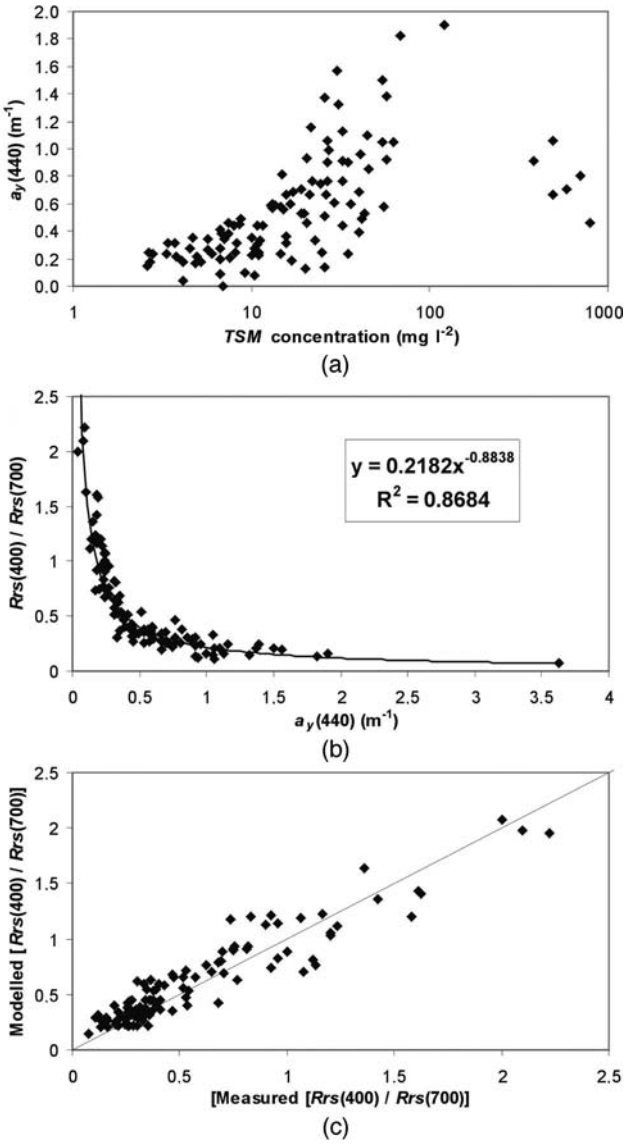

Fig. 9. (a) CDOM concentration [$a_y(440)$] as a function of the TSM concentration from in situ measurements in the Tamar estuary. (b) Empirical CDOM quantification relationships established in the Tamar estuary for the Rrs ratio 400 nm–700 nm. (c) Measured versus model (see the text for model parameter details) Rrs ratio 400 nm–700 nm.

3. Phytoplankton (Chla)

In turbid productive (lake) waters, original Chla quantification relationships were recently established by use of Rrs ratios or of the differences between Rrs ratios in the red and near-infrared spectral domains (650–750 nm), where the second Chla absorption peak is located [Fig. 2(b)].[39,40] These algorithms were tested with the Tamar data set for the following wavelengths: 675, 700, and

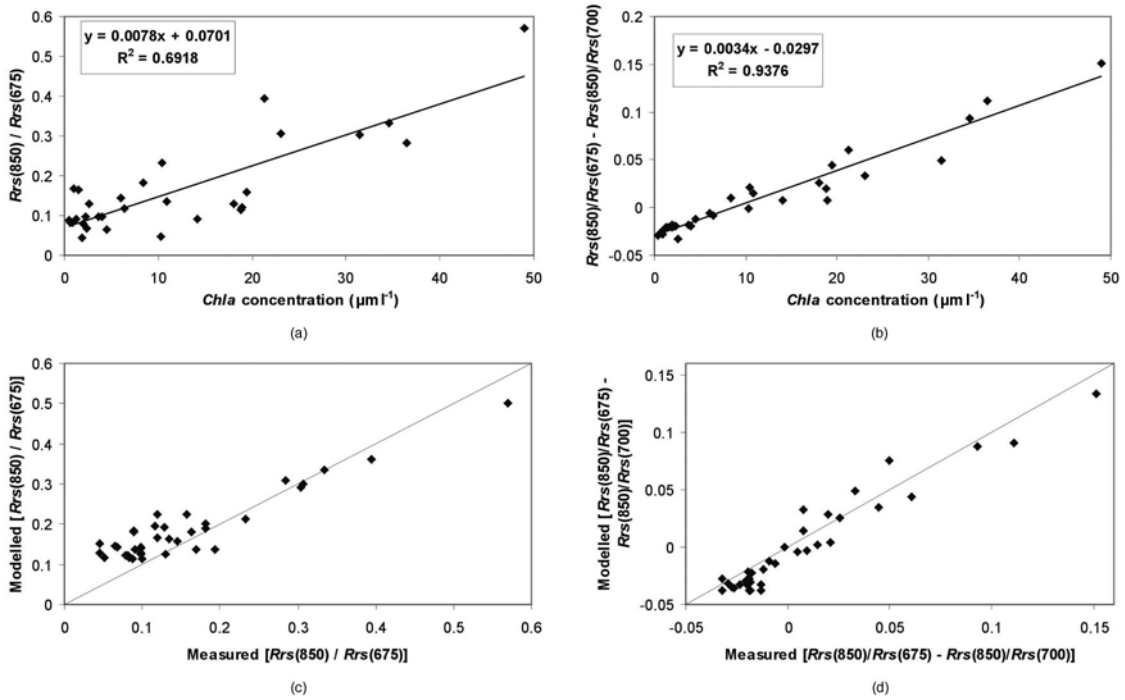

Fig. 10. Empirical Chla quantification relationships established in the Tamar estuary for (a) the Rrs ratio 850 nm–675 nm and (b) the difference between the Rrs ratios 850 nm–675 nm and 850 nm–700 nm. (c), (d) Measured versus model (see the text for model parameter details) Rrs ratio relationships for the same ratios with respect to (a) and (b).

850 nm. A simple ratio of 850 nm (where absorption by Chla is at a minimum) to 675 nm (where absorption by Chla is at a maximum) was first considered, and a correlation with *in situ* measurements was observed [Fig. 10(a)], but points were rather scattered (determination coefficient of 0.7). This ratio was obviously also affected by the NAP (concentration, optical properties). See the Rrs(850)/Rrs(650) ratio [Figs. 8(b) and 8(d).] Good results were systematically obtained when we considered a difference between specific Rrs ratios: a first ratio including the Rrs signal near 675 nm, where Chla absorption is at a maximum, minus a second ratio including the Rrs signal at a nearby wavelength (e.g., 700 nm), where Chla absorption is at a minimum [Fig. 10(b)]. The second ratio, which is mainly representative of the NAP contribution, significantly removed the NAP influence. In both cases, linear relationships with a positive slope were obtained (note that minimum Chla concentrations correspond to negative values when the difference of Rrs ratios is considered.

The model reproduced the observed relationships when the mean IOP values and the measured TSM concentrations [Figs. 10(c) and 10(d)] were considered as inputs. Considering the CDOM contribution was not necessary, as the red and near-infrared wavelengths are not significantly influenced by CDOM. The model also reproduced the empirical relationships when a constant TSM concentration taken in the range 10–100 mg l^{-1} (representative of the Tamar estuary) was applied. This result deteriorated when a significantly lower or higher constant TSM concentration (e.g., 1 or 1000 mg l^{-1}) was used. Therefore using mean IOP values and a mean TSM concentration (representative of the study area) in the model is sufficient to establish a valid Chla quantification relationship. To explain these observations, let us consider the difference of ratios Rrs(850)/Rrs(675) − Rrs(850)/Rrs(700)], denoted the Diff_ratio. Assuming low spectral variations of Q in Eq. (7), this difference can be written as

$$\mathrm{Diff\_ratio} = \frac{b_b(850)}{a(850)+b_b(850)} \Big/ \frac{b_b(675)}{a(675)+b_b(675)} - \frac{b_b(850)}{a(850)+b_b(850)} \Big/ \frac{b_b(700)}{a(700)+b_b(700)}, \tag{13}$$

$$\mathrm{Diff\_ratio} = \frac{b_b(850)}{b_b(675)} \frac{a(675)+b_b(675)}{a(850)+b_b(850)} - \frac{b_b(850)}{b_b(700)} \frac{a(700)+b_b(700)}{a(850)+b_b(850)}. \tag{14}$$

As a first approximation, the $b_b(\lambda)$ coefficient is due only to NAP backscattering properties, and spectral variations of $b_{bs}(\lambda)$ are low from 675 to 850 nm [Eq. (11)]: $b_b(\lambda) \approx b_{bs}(\lambda)$ and $b_{bs}(675) \approx b_{bs}(700) \approx b_{bs}(850)$. Equation (14) is thus simplified to

$$\text{Diff\_ratio} = \frac{a(675) + b_{bs}(675)}{a(850) + b_{bs}(850)} - \frac{a(700) + b_{bs}(700)}{a(850) + b_{bs}(850)} \approx \frac{a(675) - a(700)}{a(850) + b_{bs}(850)}. \quad (15)$$

At these wavelengths, absorption by NAP [Eq. (10)] is low compared to absorption by pure water. Absorption by Chla is significant at 675 nm (second absorption peak) but negligible at 700 nm compared to absorption by pure water [Fig. 3(b)]. Thus relation (15) can be rewritten approximately as

$$\text{Diff\_ratio} = \frac{a_w(675) + a_c(675) - a_w(700)}{a_w(850) + b_{bs}(850)} = \frac{a_c(675)}{a_w(850) + b_{bs}(850)} + \frac{a_w(675) - a_w(700)}{a_w(850) + b_{bs}(850)}. \quad (16)$$

Introducing the mass specific IOPs yields for Eq. (16)

$$\text{Diff\_ratio} = \frac{a_c^*(675)}{a_w(850) + \text{NAP}_c \times b_{bs}^*(850)}\,\text{Chla} + \frac{a_w(675) - a_w(700)}{a_w(850) + \text{NAP}_c \times b_{bs}^*(850)}. \quad (17)$$

Thus Diff_ratio would be a linear function of the Chla concentration if

$$\frac{a_c^*(675)}{a_w(850) + \text{NAP}_c \times b_{bs}^*(850)} \quad \text{(slope)},$$

$$\frac{a_c^*(675) - a_w(700)}{a_w(850) + \text{NAP}_c \times b_{bs}^*(850)} \quad \text{(offset)}$$

were constant values. The $a_w(675)$, $a_w(700)$, and $a_w(850)$ coefficients are constant values,[21,22] $b_{bs}^*(550)$ is equal to (0.0095 ± 0.0015 g m^{-1}; Table 2), and NAP_c ($\approx$TSM concentrations) corresponding to measurements reported in Fig. 10 vary in the range (2–64 mg l^{-1}). Consequently the slope and offset variations are quite limited (decrease of 11% when NAP_c increases from 2 and 64 mg l^{-1}). This explains why Diff_ratio is as a first approximation a linear function of the Chla concentration, almost independently of the NAP_c generally encountered in the Tamar surface waters. Strong light scattering by NAP (strong enough to compensate for absorption by pure water in the red and near-infrared spectral domains) is thus the condition necessary for one to detect the second Chla absorption peak (near 675 nm) and potentially quantify the Chla concentrations. This condition is fulfilled in the three estuaries, but high Chla concentrations were observed only in the Tamar estuary during our field measurements.

5. Conclusions

In three European estuaries (Gironde and Loire in France and Tamar in the UK), the water's optical properties were measured and modeled. Measurements included the Rrs signal and CDOM, NAP, and Chla absorption coefficients. A simple optical model was used to relate the Rrs signal to the IOPs, with the concentration, absorption, and backscattering coefficients of the several water constituents taken into consideration. Using Rrs ratios, we established empirical relationships to quantify the TSM concentrations in the three estuaries, with also the CDOM and Chla concentrations in the Tamar estuary.

The measured and modeled absorption coefficients were in good agreement with the values observed in various European coastal waters.[23] These coefficients exhibit significant variations within the same estuary and from one estuary to another (Table 2). It is now necessary to explain these variations from the composition and size of the water constituents; an effort will be made to do so in future studies. The model fitted backscattering coefficients used to reproduce the measured Rrs spectra were also within the range observed in European coastal waters.[26] The IOPs in the Gironde and Loire estuaries appeared to be dominated by the NAP optical properties. In the Tamar, the NAP optical properties were also globally dominant, but the contributions of CDOM (in the 400–500 nm spectral domain) and Chla (during the summer bloom) appeared to be significant. The Chla second absorption peak, centered about 675 nm allows Chla optical properties to be detected on the Rrs signal in highly turbid waters, and hence Chla concentrations can potentially be determined from remote-sensing of ocean color data.

Using a Rrs ratio between a near-infrared (e.g., 850 nm) and a visible (e.g., 550 or 650 nm) wavelength, we established robust TSM quantification relationships in each study area. Therefore the results suggest that a similar TSM quantification algorithm, with local modifications, may be developed in any turbid estuarine waters. In the Tamar estuary, the Rrs ratio from 400 to 700 nm was used to quantify the CDOM concentration; a difference between two Rrs ratios [Rrs(850)/Rrs(675) − Rrs(850)/Rrs(700)] was used to quantify the Chla concentration. These empirical relationships were well reproduced with the optical model by use of mean IOP values as inputs. Results suggest that the optical model presented can be used to develop a robust Rrs algorithm and quantify successively the TSM (thus the NAP) and then CDOM and Chla concentrations in turbid estuarine waters. The mean IOPs of the estuarine environment considered are the only model inputs required.

In situ measurements are needed to assess the variability of the NAP backscattering coefficient (magnitude and spectral slope), and additional measurements are required for validation of the Chla quantification relationship established in the Tamar estuary. Once validated, these relationships will be

applied to satellite and airborne remote-sensing data for observing the tidal and seasonal dynamics of the water constituents. The main difficulty with remote-sensing data is atmospheric correction. In turbid waters, for which the Rrs signal in red and near-infrared wavelengths is significant, the black target assumption made over ocean waters becomes invalid,[42] and therefore a well-defined knowledge of the water's optical properties in this spectral domain is required for accurate atmospheric corrections.[43] An alternative solution is to use a radiative transfer code that integrates all available metrological data as a first step in determining aerosol optical properties.[4,44]

This research was supported by a European Marie Curie fellowship (Framework 5; EVK3-CT-2002-50012) and a National Environmental Research Council (UK) small grant (NER/B/S/2002/00555, PI Lavender).

References

1. H. Siegel, M. Gerth, and A. Mutzke, "Dynamics of the Oder River plume in the Southern Baltic Sea: satellite data and numerical modelling," Cont. Shelf Res. **19,** 1143–1159 (1999).
2. R. J. Vos, P. J. G. Brummelhuis, and H. Gerritsen, "Integrated data-modelling approach for suspended sediment transport in a regional scale," Coast. Eng. **41,** 177–200 (2000).
3. International Ocean Colour Coordinating Group, "Remote sensing of ocean colour in coastal, and other optically-complex, waters," Rep. of the IOCCG (International Ocean-Colour Coordinating Group, 2000).
4. D. Doxaran, J. M. Froidefond, S. J. Lavender, and P. Castaing, "Spectral signature of highly turbid waters. Application with SPOT data to quantify suspended particulate matter concentrations," Remote Sens. Environ. **81,** 149–161 (2002).
5. D. Doxaran, J. M. Froidefond, and P. Castaing, "A reflectance band ratio used to estimate suspended matter concentrations in coastal sediment-dominated waters," Int. J. Remote Sens. **23,** 5079–5085 (2002).
6. D. Doxaran, J. M. Froidefond, and P. Castaing, "Remote sensing reflectance of turbid sediment-dominated waters. Reduction of sediment type variations and changing illumination conditions effects using reflectance ratios," Appl. Opt. **42,** 2623–2634 (2003).
7. D. Doxaran, R. C. N. Cherukuru, and S. J. Lavender, "Use of reflectance band ratios to estimate suspended and dissolved matter concentrations in estuarine waters," Int. J. Remote Sens. **26,** 1763–1769 (2005).
8. D. Doxaran, R. C. N. Cherukuru, and S. J. Lavender, "Surface reflection effects on upwelling radiance field measurements in turbid waters," J. Opt. A Pure Appl. Opt. **6,** 690–697 (2004).
9. C. D. Mobley, "Estimation of the remote-sensing reflectance from above-surface measurements," Appl. Opt. **38,** 7442–7455 (1999).
10. D. Doxaran, R. C. N. Cherukuru, S. J. Lavender, and G. F. Moore, "Use of a Spectralon panel to measure the downwelling irradiance signal: case studies and recommendations," Appl. Opt. **43,** 5981–5986 (2004).
11. T. Ohde and H. Siegel, "Use of a derivation of immersion factors for the hyperspectral TriOS radiance sensor," J. Opt. A Pure Appl. Opt. **5,** 12–14 (2003).
12. G. S. Fargion and J. L. Mueller, "Ocean optics protocols for satellite ocean colour sensor validation. Revision 2," NASA Tech. Memo. 209966, SeaWiFS Tech. Rep. Ser. (NASA Goddard Space Flight Center, 2000).
13. A. Morel, "In-water and remote sensing measurements of ocean color," Bound. Layer Meteorol. **18,** 177–201 (1980).
14. H. R. Gordon and K. Ding, "Self-shading of in-water optical measurements," Limnol. Oceanogr. **37,** 491–500 (1992).
15. E. J. Arar and G. B. Collins, "*In vitro* determination of chlorophyll *a* and pheophytin-*a* in marine and freshwater algae by fluorescence," in *Method 445.0–Revision 2* (U.S. Environmental Protection Agency, 1997).
16. S. B. Hooker, G. Zibordi, G. Lazin and S. McLean, "The SeaBOARR-98 field campaign," NASA Tech. Memo. 1999–206892, S. B. Hooker and E. R. Firestone, eds. (NASA Goddard Space Flight Center, 1999), Vol. 3.
17. S. Tassan and G. M. Ferrari, "An alternative approach to absorption measurements on aquatic particles retained on filters," Limnol. Oceanogr. **40,** 411–417 (1995).
18. G. H. Tilstone and V. Martinez-Vicente, "Analysis of 50 samples to determine the phytoplankton absorption spectra," Rep. 1, PMA contract 14 (Plymouth Marine Laboratory, Plymouth, UK, 2004).
19. R. W. Gould and R. A. Arnone, "Remote sensing estimates of inherent optical properties in a coastal environment," Remote Sens. Environ. **61,** 290–301 (1997).
20. A. Morel and B. Gentili, "Diffuse reflectance of oceanic waters. II. Bidirectional aspects," Appl. Opt. **32,** 6864–6879 (1993).
21. R. M. Pope and E. S. Fry, "Absorption spectrum (380–700 nm) of pure water. II. Integrating cavity measurements," Appl. Opt. **36,** 8710–8723 (1997).
22. G. M. Hale and M. R. Querry, "Optical constants of water in the 200 nm to 200 μm wavelength region," Appl. Opt. **12,** 555–563 (1973).
23. M. Babin, D. Stramski, G. M. Ferrari, H. Claustre, A. Bricaud, G. Obolensky, and N. Hoepffner, "Variations in the light absorption coefficients of phytoplankton, non-algal particles, and dissolved organic matter in coastal waters around Europe," J. Geophys. Res. **10,** doi:1029/2001JC000882 (2003).
24. R. C. Smith and A. Baker, "Optical properties of the clearest natural waters (200–800 nm)," Appl. Opt. **20,** 177–184 (1981).
25. F. Lahet, S. Ouillon, and P. Forget, "A three component model of ocean colour and its application in the Ebro River mouth area," Remote Sens. Environ. **72,** 181–190 (2000).
26. M. Babin, A. Morel, V. Fournier-Sicre, F. Fell, and D. Stramski, "Light scattering properties of marine particles in coastal and oceanic waters as related to the particle mass concentration," Limnol. Oceanogr. **48,** 843–859 (2003).
27. A. Morel, "Diffusion de la lumière par les eaux de mer. Résultats expérimentaux et approche théorique," in *Optics of the Sea,* Vol. 61 of AGARD Lectures Series (Advisory Group for Aerospace Research and Development, Paris, 1973), pp. 3.1.1–3.1.76.
28. G. Abril, H. Etcheber, P. Le Hir, P. Bassoullet, B. Boutier, and M. Frankignoulle, "Oxic/anoxic oscillations and organic carbon mineralization in an estuarine maximum turbidity zone (The Gironde, France)," Limnol. Oceanogr. **44,** 1304–1315 (1999).
29. X. Irigoien and J. Castel, "Light limitation and distribution of chlorophyll pigments in a highly turbid estuary: The Gironde (SW France)," Estuar. Coast. Shelf Sci. **44,** 507–517 (1997).
30. D. G. Bowers, G. E. L. Harker, and B. Stephan, "Absorption spectra of inorganic particles in the Irish Sea and their relevance to remote sensing of chlorophyll," Int. J. Remote Sens. **17,** 2449–2460 (1996).
31. A. E. J. Miller, "Seasonal investigations of dissolved organic carbon dynamics in the Tamar estuary, U.K.," Estuar. Coast. Shelf Sci. **49,** 891–908 (1999).

32. T. J. Petzold, "Volume scattering functions for selected ocean waters," in *Light in the Sea,* J. E. Tyler, ed. (Dowden, Hutchinson, and Ross, 1972) pp. 150–174.
33. G. J. C. Underwood and J. Kromkamp, "Primary production by phytoplankton and microphytobenthos in estuaries," Adv. Ecol. Res. **29,** 93–153 (1999).
34. M. Babin and D. Stramski, "Variations in the mass-specific absoprtion coefficient of mineral particles suspended in water," Limnol. Oceanogr. **49,** 756–767 (2004).
35. S. B. Wozniak and D. Stramski, "Modeling the optical properties of mineral particles suspended in seawater and their influence on ocean reflectance and chlorophyll estimation from remote sensing algorithms," Appl. Opt. **43,** 3489–3503 (2005).
36. P. Forget, S. Ouillon, F. Lahet, and P. Broche, "Inversion of reflectance spectra of nonchlorophyllous turbid coastal waters," Remote Sens. Environ. **68,** 264–272 (1999).
37. C. D. Mobley, *Light and Water: Radiative Transfer in Natural Waters* (Academic, 1994).
38. Z. P. Lee, K. L. Carder, R. K. Hawes, R. G. Steward, T. G. Peacock, and C. O. Davis, "Model for the interpretation of hyperspectral remote-sensing reflectance," Appl. Opt. **33,** 5721–5732 (1994).
39. G. Dall'Olmo, A. A. Gitelson, and D. C. Rundquist, "Towards a unified approach for remote estimation of chlorophyll-*a* in both terrestrial vegetation and turbid productive waters," Geophys. Res. Lett. **30,** 10.1029/2003GL018065 (2003).
40. G. Dall'Olmo and A. A. Gitelson, "Effect of the variability of bio-optical parameters on the remote estimation of chlorophyll-*a* concentration in turbid productive waters: experimental results," Appl. Opt. **44,** 412–422 (2005).
41. E. J. D'Sa and R. L. Miller, "Bio-optical properties in waters influenced by the Mississippi River during low flow conditions," Remote Sens. Environ. **84,** 538–549 (2003).
42. P. S. Chavez, "An improved dark-object subtraction technique for atmospheric scattering correction of multispectral data," Remote Sens. Environ. **24,** 459–479 (1988).
43. G. F. Moore, J. Aiken, and S. J. Lavender, "The atmospheric correction of water colour and the quantitative retrieval of suspended particulate matter in Case II waters: application to MERIS," Int. J. Remote Sens. **20,** 1713–1733 (1999).
44. D. Doxaran, P. Castaing, and S. J. Lavender, "Monitoring the maximum turbidity zone and detecting fine-scale turbidity features in the Gironde estuary using high spatial resolution satellite sensor (SPOT HRV, Landsat ETM+) data," submitted to Int. J. Remote Sens.